



## Effects of Submarine Groundwater on Nutrient Concentration and Primary Production in a Deep Bay of the Japan Sea

Menghong Dong<sup>1</sup>, Xinyu Guo<sup>2\*</sup>, Takuya Matsuura<sup>3</sup>, Taichi Tebakari<sup>4</sup>, and Jing Zhang<sup>5</sup>

<sup>1</sup>State Key Laboratory of Satellite Ocean Environment Dynamics, Second Institute of Oceanography, Ministry of Natural Resources, Hangzhou, China

<sup>2</sup>Center for Marine Environmental Studies, Ehime University, Matsuyama, Japan

<sup>3</sup>Graduate Faculty of Interdisciplinary Research Faculty of Engineering, Civil Engineering and Environmental Engineering, Yamanashi University, Koufu, Japan

<sup>4</sup>Civil, Human and Environmental Science and Engineering Course, Graduate School of Science and Engineering, Chuo University, Tokyo, Japan

<sup>5</sup>Faculty of Science, Academic Assembly, University of Toyama, Toyama, Japan

*Correspondence to:* Xinyu Guo (guo.xinyu.mz@chime-u.ac.jp), ORCID ID: 0000-0002-4832-8625

**Abstract.** We constructed a coupled physical-ecosystem model with a tracking module to evaluate the influence of submarine groundwater discharge (SGD) and river water on nutrient distribution and phytoplankton growth in Toyama Bay, a deep bay in the Japan Sea. The tracking technique allows us to distinguish SGD- and river-derived nutrients in the bay and evaluate their contributions to the nutrient inventory and phytoplankton growth. Horizontally, SGD-derived nutrients were primarily distributed within a narrow band from the coastline (< 3 km), and vertically, they were abundant in the middle and bottom layers. Because of the buoyancy of SGD, SGD-derived nutrients were transported upward to the surface layer and used by the phytoplankton growth. On the other hand, river water exerted a greater effect on phytoplankton growth than SGD did, on both the spatial range and the amount of phytoplankton biomass. Due to the different distributions of river- and SGD-derived nutrients, their proportions used by phytoplankton differed from coastal to offshore areas. These findings enhance our understanding of the coastal ecosystems affected by land water.

### 1 Introduction

Submarine groundwater discharge (SGD) is a process that involves the release of groundwater from the seafloor into a coastal sea (Burnett et al., 2003; Moore, 2010). Based on the monitoring of radioactive elements such as radium and radon, the occurrence of SGD in coastal seas is well established. It was also suggested that SGD is a pathway by which freshwater and nutrients from the terrestrial groundwater system enter the marine environment (Hatta & Zhang, 2013; Lecher & Mackey, 2018; Luijendijk et al., 2020; Moore, 1996; Müller et al., 2023; Santos et al., 2021; Wang et al., 2018). The global amount of SGD is estimated to be as high as 6–7% of total surface water input to the world ocean system (Zektser, 2000) or as high as 10% of river discharge in the world ocean system (Burnett et al., 2001; Taniguchi et al., 2002).

Owing to the high nutrient concentration of groundwater, it was suggested that SGD is accompanied by the release of large amounts of nutrients into the coastal sea (Burnett et al., 2001, 2003; Church, 1996; Rodellas et al., 2015; Taniguchi et al., 2002; Wang et al., 2014; Zhang & Satake, 2003). Local- and global-scale assessments of SGD suggested that in coastal areas, SGD-derived nutrient inputs are comparable to or even higher than river-derived nutrient loads (Hatta et al., 2005; Cho et al., 2018; Zhang et al., 2020). Such significant SGD inputs can influence nutrient budgets and initiate phytoplankton blooms in the sea (Lapointe et al., 1990). Based on high Chlorophyll concentrations at sites with high SGD, Santos et al. (2021), in a report that summarized the impact of SGD-related nutrients on marine ecosystems, noted that the most documented response to SGD-derived nutrients is an increase in phytoplankton growth (Hwang et al., 2005; Taylor et al., 2006).

Two major concerns are associated with the interpretation of SGD-related observations. First, confirming the distribution of SGD-derived nutrients in the coastal seas is challenging, even though we know these nutrients are released at the sea bottom.



In coastal seas, in addition to SGD-derived nutrients, river water also inputs nutrients. To distinguish the nutrients from different sources is challenging in the observations as river water and SGD eventually mix. The second one is that it remains unclear how much of the SGD-derived nutrients is consumed by phytoplankton. In principle, SGD-derived nutrients influence phytoplankton growth only after reaching the euphotic layer. Most previous observations on SGD were carried out on the seas with a water depth < 10 m. In such shallow seas, owing to wind- or tide-induced mixing, SGD-derived nutrients are considered to easily reach the surface layer where there is sufficient sunlight (Bratton, 2010; Jiao and Post, 2019; Müller et al., 2023). However, it was also reported that sometimes drastic changes in the water column above SGD sites also make it difficult to confirm the response of phytoplankton growth to SGD-derived nutrients (Sugimoto et al., 2017). On the other hand, for the SGD released at the deep seafloor, the effects of wind- and tide-induced mixing are limited and the sunlight required for phytoplankton growth at depths where the SGD can reach may be insufficient for primary production (Cloern et al., 2014). Therefore, the second concern is particularly serious for the deep coastal seas.

The interest in knowing the effects of different origins of nutrients in the marine ecosystem is not limited to SGD. As a useful tool, the implementation of a tracking module in the ecosystem simulation to track nutrients from different sources has been proposed (Kawamiya, 2001; Ménesguen et al., 2006). This technique has been successfully applied in the Baltic Sea (Neumann, 2007), the Japan Sea (Onitsuka et al., 2007), the East China Sea (Zhang et al., 2019), and the Seto Inland Sea (Leng et al., 2023). Thus, a comprehensive evaluation of SGD and its impacts on the marine ecosystem, which is urgently required, is possible by applying such a numerical ecosystem model with a tracking module. Comparing the contributions of SGD-derived nutrients with those of nutrients from other land-side-derived sources such as river water to phytoplankton growth will enhance understanding regarding the integrated land-sea nutrient cycle and ecosystem.

Here, we selected Toyama Bay, a deep bay in the Japan Sea (Figure 1a), as our study area. This bay is characterized by a narrow continental shelf and steep slopes, with a trough across the continental shelf and a slope toward the inner part of the bay (Figure 1b). On the land side of the bay, there are many mountains up to 3,000 m in height. These mountains are characterized by steep slopes from the mountains to the coast. Further, large amounts of freshwater flow into this bay during the snowmelt season (Watanabe et al., 2013). This bay is ideal for studying SGD because it is easily accessible and has several SGD sites off the eastern coastal area. These SGD sites are distributed from the shore to relatively deep waters (Hatta & Zhang, 2013; Koyama et al., 2005; Nakaguchi et al., 2005; Zhang et al., 2005; Zhang & Satake, 2003). The reported SGD flow rates are greater in this area than in most areas worldwide (Taniguchi et al., 2002; Zhang et al., 2005). Specifically, the SGD in this area is estimated to be ~13–20% of the river water discharge into the bay (Hatta et al., 2005; Hatta and Zhang, 2013). It was also shown that SGD-derived nutrient loading in this area is slightly higher than riverine nutrient inputs (Hatta et al., 2005).

To investigate the spatiotemporal distribution of SGD-derived nutrients and clarify their contribution to the phytoplankton growth in the bay, we developed a coupled physical-ecosystem model that covers the entire Toyama Bay area and takes into account SGD and riverine nutrient inputs. We used the numerical model to investigate the nutrient dynamics and marine ecosystem structure of this bay. Further, using the tracking technique implemented in the model, we examined the distribution of SGD-derived nutrients and nutrients from other sources and evaluated their contributions to the nutrient inventory and phytoplankton growth. Finally, we examined the importance of the buoyancy effect of SGD in controlling the upward transport of SGD-derived nutrients.

## 2 Model configuration

### 2.1 Hydrodynamic model

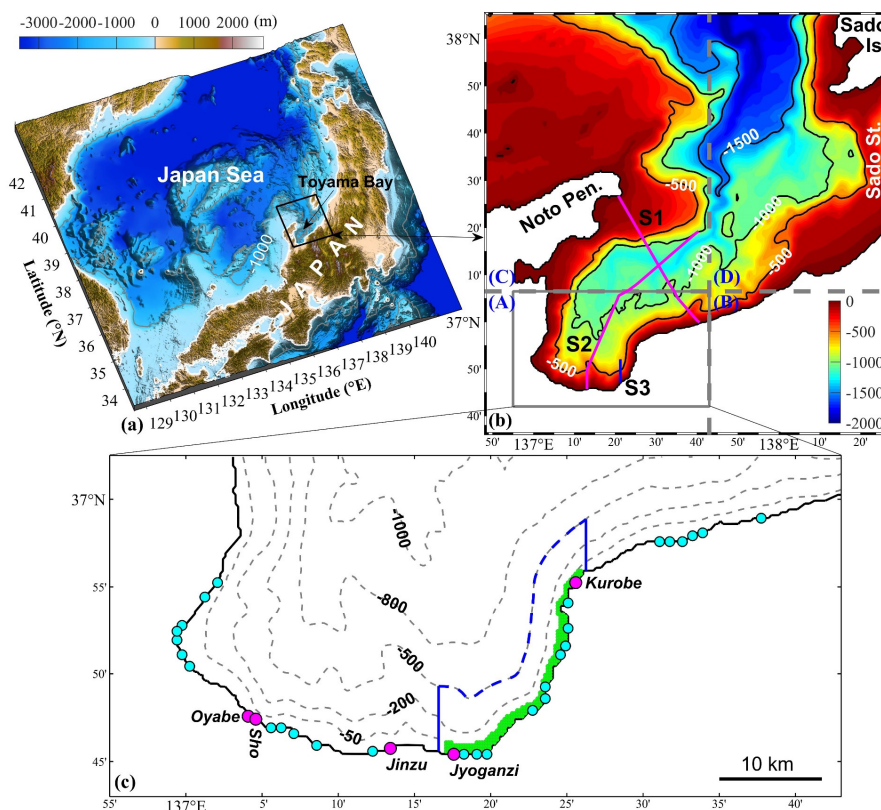
In this study, we used the Stony Brook Parallel Ocean Model (sbPOM), a parallel version of the Princeton Ocean Model as the hydrodynamic model. Some additional information on this model is provided in Text S1. The model domain covers an area of approximately 150 km × 150 km including Toyama Bay (Figure 1b). Given that the inner part of the bay is considerably



affected by freshwater input and the sizes of the river mouths along the coast are relatively small, we used a variable grid system with a fine resolution in the inner part and a coarse resolution in the outer part. In the inner part (area (A) in Figure 1b), the grid size is 10 seconds (~300 m) in the zonal and meridional directions. In the other three areas, the grid size is 30 seconds (zonal) x 10 seconds (meridional) in area (B), 10 seconds (zonal) x 30 seconds (meridional) in area (C), and 30 seconds (both zonal and meridional) in area (D). To avoid an abrupt change in grid size, we set a transition zone of ~5.5 km between the areas of 10'' and 30''. In the vertical direction, there are 31 sigma layers, and the vertical level range is fine near the surface layer. The topography used in the model is based on the 30-second topography data (JTOPO30) prepared by the Marine Information Research Center (MIRC), Japan Hydrographic Association. Two modifications were made to the original topography data: setting the minimum (5 m) depth in the model and smoothing the topography data to satisfy the following criteria (Mellor et al., 1994):

$$\frac{|H_{i+1}-H_i|}{(H_{i+1}+H_i)} \leq \alpha, \tag{1}$$

where  $H_{i+1}$  and  $H_i$  are the depths at two adjacent grids, and  $\alpha$  is a slope factor equal to 0.2.



95

**Figure 1:** (a) Study area. (b) Model domain for Toyama Bay. Colors indicate the water depth. The model domain was divided into four areas from (A) to (D) with different horizontal resolutions. The respective horizontal resolutions are (1) 300 m × 300 m, (2) 900 m × 300 m, (3) 300 m × 900 m, and (4) 900 m × 900 m. “Pen.,” “Is.,” and “St.” is the abbreviation of Peninsula, Island, and Strait respectively. The three lines S1, S2, and S3 represent the sections to show vertical distributions of the results. (c) The inner part of the bay. The circles indicate river mouths that supply freshwater and nutrients, with pink for first-class rivers and blue for second-class rivers. The green area means the location of submarine groundwater discharge (SGD). The area inside the blue lines is used to calculate the inventories and material flows of SGD- and river-derived nutrients.

100

The model was driven by forces at the surface boundary and lateral boundary. The surface forcing was calculated based on the hourly output of the grid point value of the mesoscale model (GPV-MSM) provided by the Japan Meteorological Agency (Grid

105



Point Value of Meso-Scale Model) with a resolution of  $1/16^\circ$  in zonal direction and  $1/20^\circ$  in meridional direction. The surface wind stress was calculated based on the difference of 10-m height wind velocity from GPV-MSM and the surface current velocity from our hydrodynamic model with the drag coefficient given by Mellor and Blumberg (2004). The surface heat flux consists of four terms: shortwave radiation, longwave radiation, sensible heat flux, and latent heat flux. The surface shortwave radiation was calculated utilizing the cloud cover data from the GPV-MSM and the formula in Rosati and Miyakoda (1988). The downward penetration of the shortwave radiation was calculated by the analytical formula given by Paulson and Simpson (1977). The longwave radiation, latent heat flux, and sensible heat flux were calculated by the bulk formula given by Kondo (1975) using the 1.5-m air temperature, 1.5-m relative humidity, cloud cover, 10-m wind speed data from the GPV-MSM, and the sea surface temperature from our hydrodynamic model. In addition, the precipitation from the GPV-MSM was specified in the model.

The lateral boundary conditions at the Japan Sea side, including surface elevation, current velocity, temperature, and salinity, were obtained by the bilinear interpolation of daily model output from the Japan Coastal Ocean Predictability Experiment (JCOPE-T) system developed by the Japan Agency for Marine-Earth Science and Technology (JAMSTEC) with a resolution of  $1/36^\circ$  in both zonal and meridional directions (Varlamov et al., 2010). The lateral boundary conditions at the land side are the river discharges and SGD. We specified the discharges of five first-class and 28 second-class rivers, whose daily values were obtained from a terrestrial hydrology model developed by the River Engineering and Hydrology Laboratory, Chuo University (Matsuura and Tebakari, 2022). This model reproduced both the seasonal variations and the short-term fluctuations (Figure 2a). The mean value of the total river discharge into the bay is  $295.4 \text{ m}^3 \text{ s}^{-1}$ , in which the first-class rivers accounted for approximately 78% (Figure 2a).

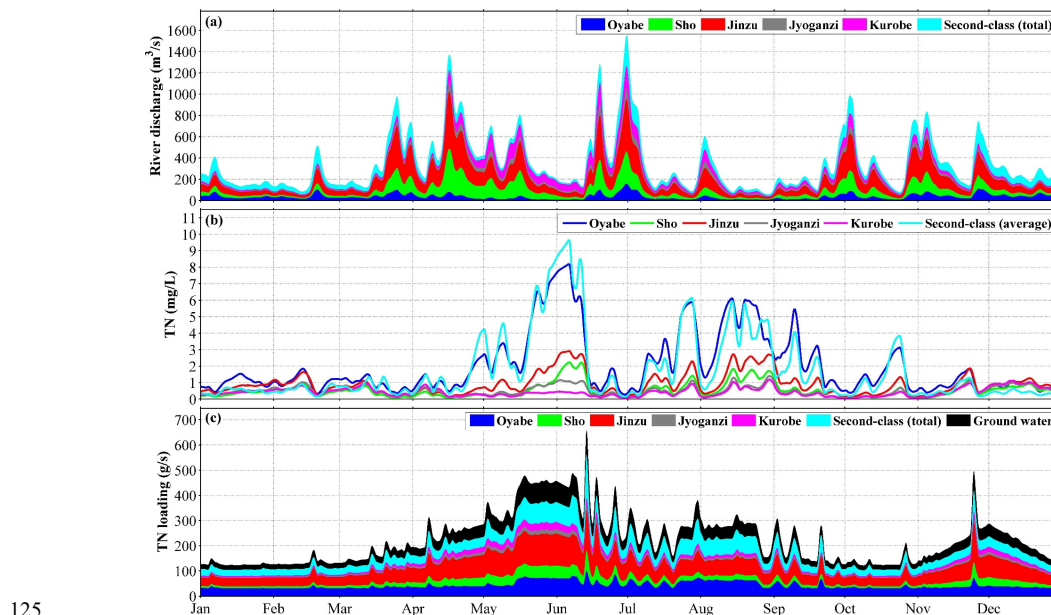


**Figure 2: (a) River discharge in 2016, (b) Total nitrogen (TN) concentration in the rivers, (c) TN loading from rivers. Dissolved inorganic nitrogen (DIN) concentration was specified to be 70% of TN concentration.**

Given that SGD predominantly occurs in the eastern coastal area of the bay (Hatta and Zhang, 2013), we set the outlet location of SGD at the sea bottom in an area between the Joganzi and Kurobe Rivers and between the coastline and the 70-m isobath (Figure 1c). The SGD amount into the bay is estimated to be 15% of the total discharge of nearby rivers, including the Joganzi and Kurobe Rivers, and 10 second-class rivers (Hatta et al., 2005; Hatta and Zhang, 2013) and has the same temporal variation as the river discharges. Consequently, we obtained a mean SGD of  $12.6 \text{ m}^3 \text{ s}^{-1}$ . The corresponding flow velocity of SGD is



about  $5.7 \text{ cm day}^{-1}$ , which is consistent with previous observations (Zhang et al., 2005). Because this value is small, we did not consider its mass contribution to the bay. However, we included its buoyancy effect by extracting a bottom flux of salinity with a formula  $RS_b$ , where  $R$  is the amount of SGD and  $S_b$  is the bottom salinity. As we will show later, introducing the SGD's buoyancy effect is a key to the upward movement of the SGD-derived nutrients.

The model was run for two years (2015-2016) from the rest state with initial temperature and salinity fields interpolated from the JCOPE-T. We treated 2015 as a spin-up and used the results of 2016 for our analysis.

## 140 2.2 Ecosystem model

To simulate seasonal variations in nutrients, phytoplankton, zooplankton, and detritus (NPZD), we used an NPZD-type model, which has been used to simulate seasonal variations in nutrient and primary production in the Japan Sea (Onitsuka et al., 2007; Onitsuka and Yanagi, 2005). This nitrogen-based model has a similar structure to that of Fasham et al. (1990). The reason for choosing this ecosystem model is provided in Text S2. It comprises five compartments, namely, dissolved inorganic nitrogen (DIN), dissolved inorganic phosphate (DIP), phytoplankton (PHY), zooplankton (ZOO), and detritus (DET). The five biological compartments obey the same advection and diffusion equations as the water temperature but have an additional term representing biogeochemical processes, as follows:

$$\frac{\partial C}{\partial t} + Adv(C) = Diff(C) + Bio(C), \quad (2)$$

$$Adv(C) = u \frac{\partial C}{\partial x} + v \frac{\partial C}{\partial y} + w \frac{\partial C}{\partial z}, \quad (3)$$

$$150 \quad Diff(C) = \frac{\partial}{\partial x} \left( K_h \frac{\partial C}{\partial x} \right) + \frac{\partial}{\partial y} \left( K_h \frac{\partial C}{\partial y} \right) + \frac{\partial}{\partial z} \left( K_v \frac{\partial C}{\partial z} \right), \quad (4)$$

where  $C$  is the concentration of a state variable,  $t$  is time,  $Adv(C)$  is the advection term in which  $u$ ,  $v$ ,  $w$  are velocity components in three directions ( $x$ ,  $y$ ,  $z$ ),  $Diff(C)$  is the diffusion term, and  $Bio(C)$  is the sum of all the biogeochemical processes, which follow the equations in Guo and Yanagi (1998).  $K_h$  and  $K_v$  represent the horizontal and vertical eddy diffusivities, respectively. A schematic diagram of the biogeochemical processes between these state variables is provided in Figure S1 and the equations for the biogeochemical processes are provided in Text S3. The parameters used in the ecosystem model were obtained from previous studies (Guo and Yanagi, 1998; Ishizu et al., 2019; Onitsuka et al., 2007; Onitsuka and Yanagi, 2005) and modified slightly as shown in Table 1.

The initial and open boundary conditions for the ecosystem model were from the monthly results of a biogeochemical and carbon model (JCOPE\_EC) for the Japan Sea and the North Western Pacific (Ishizu et al., 2019), which was based on the Japan Coastal Ocean Predictability Experiment 2 (JCOPE2) system with a horizontal resolution of  $1/12^\circ$  (Miyazawa et al., 2009).

The nutrient (DIN and DIP) loadings (Figure 2c) of the rivers were calculated using river discharge (Figure 2a) and nutrient concentration (Figure 2b) obtained from a terrestrial hydrology model (Matsuura et al., 2023). The ratio of nitrate to phosphate in all rivers has a mean value of 17.8, which is a little larger than the Redfield ratio (N: P=16:1) (Redfield et al., 1963). The DIN loading of the first-class rivers accounts for approximately 78% of the total riverine DIN loading, and the mean value of the total DIN loading is  $133.4 \text{ g s}^{-1}$ . The total DIN loading shows a clear seasonal variation, with high values in June and July and low values in January (Figure 2c). The SGD nutrient loading was considered to be the same as the sum of the nutrient loading of nearby rivers and kept the same N:P ratio (= the Joganzi and Kurobe Rivers and 10 second-class rivers) (Hatta et al., 2005) whose mean value of DIN was  $26.7 \text{ g s}^{-1}$ , which is approximately 20% of the total riverine nutrient loading.

The coupled physical-ecosystem model was initiated on the first day of January 2015 and subsequently integrated for 2 years. The first year was treated as the spin-up of the ecosystem model, while the second year, when the model results showed a stable seasonal variation, was analyzed.



**Table 1: Parameters used in the Ecosystem model.**

| Symbol     | Definition  | Value  | Unit                      |
|------------|---|--------|---------------------------|
| $V_{max}$  | Maximum photosynthetic rate of PHY at 0 °C          | 1.5    | $d^{-1}$                  |
| $K_{DIN}$  | Half saturation constant of PHY for DIN             | 4.5    | $mmolN\ m^{-3}$           |
| $K_{DIP}$  | Half saturation constant of PHY for DIP             | 0.12   | $mmolN\ m^{-3}$           |
| $I_{opt}$  | Optimum light intensity                             | 95     | $W\ m^{-2}$               |
| $k_{pho}$  | Temperature coefficient for the photosynthetic rate | 0.0693 | $^{\circ}C^{-1}$          |
| $\alpha_1$ | Light dissipation coefficient of seawater           | 0.015  | $m^{-1}$                  |
| $\alpha_2$ | Self-shading coefficient of PHY                     | 0.054  | $m^2\ mmolN^{-1}$         |
| $P_{res}$  | Respiration rate of PHY at 0 °C                     | 0.03   | $d^{-1}$                  |
| $k_{res}$  | Temperature coefficient for respiration             | 0.0519 | $^{\circ}C^{-1}$          |
| $P_{mor}$  | Mortality rate of PHY at 0 °C                       | 0.2    | $m^3\ mmolN^{-1}\ d^{-1}$ |
| $k_{mor1}$ | Temperature coefficient for PHY mortality           | 0.0693 | $^{\circ}C^{-1}$          |
| $G_{max}$  | Maximum grazing rate of ZOO at 0 °C                 | 0.3    | $d^{-1}$                  |
| $\lambda$  | Ivlev constant of ZOO                               | 1.4    | $m^3\ mmolN^{-1}$         |
| $\sigma$   | The threshold value for grazing PHY                 | 0.043  | $mmolN\ m^{-3}$           |
| $k_{gra}$  | Temperature coefficient for grazing                 | 0.0693 | $^{\circ}C^{-1}$          |
| $Z_{mor}$  | Mortality rate of ZOO at 0 °C                       | 0.07   | $m^3\ mmolN^{-1}\ d^{-1}$ |
| $k_{mor2}$ | Temperature coefficient for ZOO mortality           | 0.0693 | $^{\circ}C^{-1}$          |
| $\alpha_Z$ | Assimilation efficiency of ZOO                      | 0.7    | Non-dimensional           |
| $\beta_Z$  | Growth efficiency of ZOO                            | 0.3    | Non-dimensional           |
| $D_{dec}$  | Decomposition rate of DET at 0 °C                   | 0.15   | $d^{-1}$                  |
| $k_{dec}$  | Temperature coefficient for decomposition           | 0.0693 | $^{\circ}C^{-1}$          |
| $S_{PHY}$  | Sinking velocity of PHY                             | 0.1    | $m\ d^{-1}$               |
| $S_{DET}$  | Sinking velocity of DET                             | 5      | $m\ d^{-1}$               |
| C/chl.a    | The ratio of carbon to Chlorophyll-a                | 50     | Non-dimensional           |
| C/N        | Redfield ratio                                      | 106/16 | Non-dimensional           |

175

### 2.3 Tracking module

To evaluate the respective contributions of external nutrients to total nutrient and primary production in the bay, a tracking module was embedded into the coupled physical-ecosystem model (Kawamiya, 2001; Ménesguen et al., 2006). In this tracking module, the state variables for different nutrient sources were calculated separately as was done in the original physical-ecosystem model. Because the primary production in the Japan Sea is primarily limited by nitrogen (Onitsuka and Yanagi, 2005), the tracking module was established for nitrogen.

180

In our study area, we considered three external nutrient sources: the Japan Sea (JS), rivers (RV), and SGD (GW). As an example for SGD, we used  $DIN_{GW}$ ,  $PHY_{GW}$ ,  $ZOO_{GW}$ , and  $DET_{GW}$  to track the cycle of SGD-derived nutrients in the system.

185

The difference between total nutrients to the sum of these three external nutrients was considered as residual nutrients (RE), which was also calculated because its disappearance means the perfect representation of JS, RV, and SGD for the nutrients in our study area.



In the calculation, each subset of variables was attributed to the same physical and biogeochemical processes as was the case for total nutrients. It has the same advection and diffusion terms as the total nutrients but with different boundary conditions that will be described later. The separation of biogeochemical terms was based on the ratio of one subset state variable to the sum of the same state variables in the original ecosystem model. For example, the term for one biogeochemical process from state variable A to state variable B, named  $Bio^{A \rightarrow B}$  (A and B can be any of four state variables, i.e., DIN, PHY, ZOO, and DET), in the original ecosystem model, was separated using the ratio of state variable A in the process supported by a single nutrient source,  $A_X$  (X represents any of JS, RV, GW, and RE) to the state variable A as a whole in the original ecosystem model, as described in Eq. (5).

$$195 \quad Bio_X^{A \rightarrow B} = \frac{[A_X]}{[A]} \cdot Bio^{A \rightarrow B}, X = JS, RV, GW, RE \quad (5)$$

where  $Bio_X^{A \rightarrow B}$  represents the biogeochemical process supported by a single source of nutrients. The brackets denote concentrations, with  $[A]$  representing the sum of  $[A_{JS}]$ ,  $[A_{RV}]$ ,  $[A_{GW}]$ , and  $[A_{RE}]$ . The complete expression for each biogeochemical process supported by a single nutrient source in the tracking module is provided in Text S4.

The tracking module was integrated simultaneously with the coupled physical-ecosystem model for all the nutrients. The initial conditions for the concentration of the subset state variables corresponding to the three external nutrient sources were set to zero while those for the residual nutrients were the results of the coupled physical-ecosystem model for all the nutrients. For the tracking calculation of the rivers and SGD-derived nutrients, we introduced their nutrient fluxes from the rivers and SGD, respectively; both processes have no nutrient fluxes from the Japan Sea at the open boundaries. For the tracking calculation of the nutrients from the Japan Sea, it has the only supply from the open boundaries; for the tracking calculation of the residual nutrients, it has zero supply from rivers, SDG, and the open boundaries. The other configurations for the tracking module were the same as those for the original ecosystem model. The integrations for each tracking process also lasted for two years to obtain a stable seasonal variation state.

### 3 Results

The results of the physical-ecosystem model were validated by the observational data, including temperature, salinity, DIN, and Chlorophyll-a concentration from the Marine Information Research Centre (MIRC) Ocean Dataset 2005, provided by the MIRC, Japan Hydrographic Association (MIRC, 2005). The original data were collected from 1934 to 2001, and the spatial-temporal coverage of data was higher for temperature and salinity than for DIN and Chlorophyll-a. We processed the original data to the standard layer depth and averaged the data spatially following the model grid and temporally following the month. The gridded monthly climatological data were then compared with the model results. The positions of the observational data are plotted along with the surface distributions of model results (Figure 3).

The correlation coefficients and root mean square deviations (RMSD) between the observational data and the model results in different months are listed in Table S1. The mean correlation coefficients (RMSD) of temperature, salinity, DIN, and Chlorophyll-a in all months are 0.92 (1.75 °C), 0.64 (0.26), 0.93 (2.25 mmolN m<sup>-3</sup>), and 0.65 (0.13 mg m<sup>-3</sup>), respectively. The comparisons for different depths are shown in the scatter plots (Figures S2a–S2d), which indicate that the model results, including the spatial distributions and seasonal variations of the physical and biological fields, were in good agreement with the observational data.

#### 3.1 Physical fields

The eastward coastal branch of the Tsushima Warm Current (TWC) flows into the upper layer of Toyama Bay, and the inflow shows two patterns within the year. From April to August, it enters the bay along the west coast, resulting in higher salinity in the western part of the bay, whereas in other months, it tends to flow southeastward across the bay mouth (Figures 3 and S3).



These two inflow patterns are consistent with those reported by previous studies (Igeta et al., 2017, 2021; Nakada et al., 2005). Additionally, the surface flow pattern in the inner part of the bay is counterclockwise along the coast from west to east (Figure S3).

Affected by the inflow of freshwater from the land side, the surface salinity in the inner part of the bay is always low, and the low salinity surface water spreads out along the eastern coast (Figure 3). In April, the freshwater discharge increases with the melting of snow (Figure 2a), which increases the area of low-salinity surface water in the bay. Then, with the entry of the high-salinity coastal branch of the TWC along the western coast, the low-salinity surface water is concentrated in the eastern part of the bay. With the second increase in freshwater discharge in July, the area of the low-salinity water expands again (Figure 3). In the following month toward the winter, the low-salinity surface water begins to mix downward, reaching about 200 m in January (Figures 4 and S4). The low-salinity water can spread out to the outer part of the bay and even distribute near the Sado Strait (Figure 1) along the eastern coast (Figures 3 and 4). The intrusion of the high-salinity water from the TWC in the intermediate layer from the subsurface to about 200 m begins in May and continues until December (Figure 4).

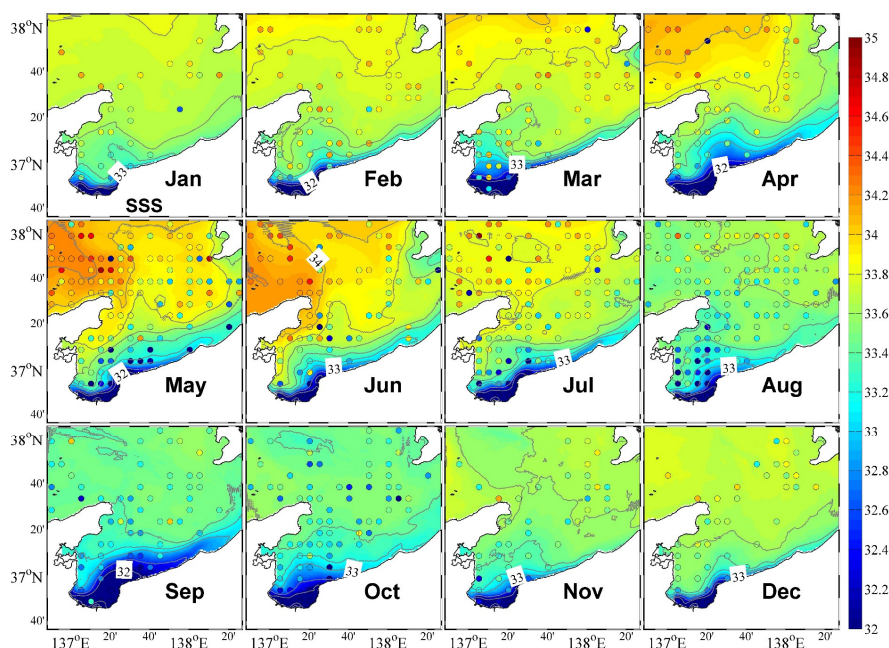
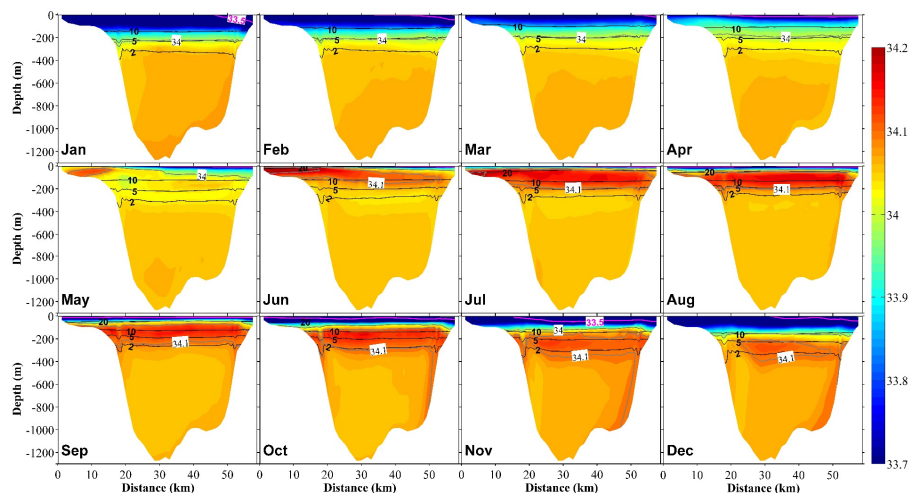


Figure 3: Monthly mean surface salinity. The circles represent observational data, whose color bar is shown on the right.

240





**Figure 4:** Vertical distribution at section S1 (Figure 1b) of salinity (color) and temperature (black contours) in 12 months. The pink contour line represents a salinity of 33.5.

245 The water temperature in the upper layer (0-200 m) shows remarkable seasonal variations, which are stratified in summer (starting from May) and mixed in winter (starting from October). Below the middle layer (>200 m), a permanent thermocline exists (Figure 4). The water in the bay consists of three different water masses, namely, the coastal surface layer (< 50 m), with low salinity resulting from the freshwater discharge into the bay from rivers; the TWC water mass (at a depth of ~200 m) with high salinity; and the deep water mass (Japan Sea Proper water).

### 250 3.2 Biological fields

Our model showed that the surface distribution of DIN was similar to that of the low-salinity surface water (Figure 5), and the vertical distribution of DIN in the central part of the bay showed open-ocean characteristics, with low and high nutrient concentrations in the surface and lower layers, respectively. Further, we also consistently obtained high nutrient concentrations along the inner coastal area of the bay throughout the year (Figures 5 and S5). From winter to spring, the upward supply of nutrients from the lower layer owing to vertical mixing promoted the increase of nutrients in the surface layer (Figure S5), which is a necessary condition for the appearance of phytoplankton spring bloom.

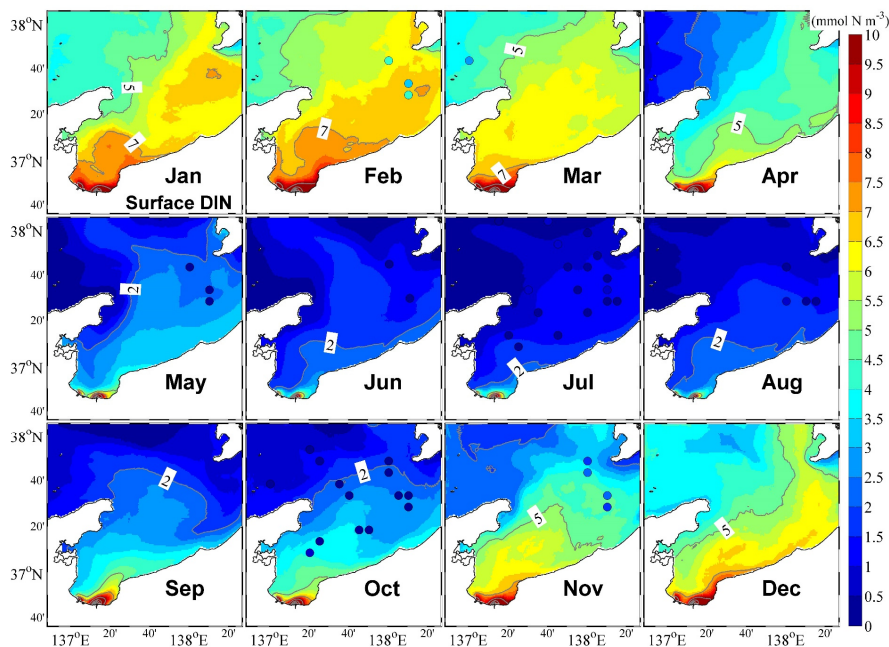


**Figure 5: Monthly mean surface dissolved inorganic nitrogen (DIN). The color circles represent observational data.**

260 Our observations also indicated that in the central bay area, phytoplankton are primarily distributed in the upper 100-m layer, with the upper 50-m layer characterized by a remarkable spring bloom with a high abundance of phytoplankton (Figures 6 and 7). From May, surface phytoplankton abundance decreased throughout the bay, except in the estuary area where nutrients are supplied from the landside (Figure 6). Further, in May, the maximum subsurface chlorophyll concentration, which persisted till September, was observed at a depth of approximately 30 m (Figure 7). From late autumn to winter, the growth of

265 phytoplankton is restricted due to light and temperature limitations, causing a decrease in the concentration of phytoplankton in the whole area (Figures 6 and 7). The decrease in phytoplankton during this period promotes nutrients from the rivers to accumulate in the estuary area (Figures 5 and S5).

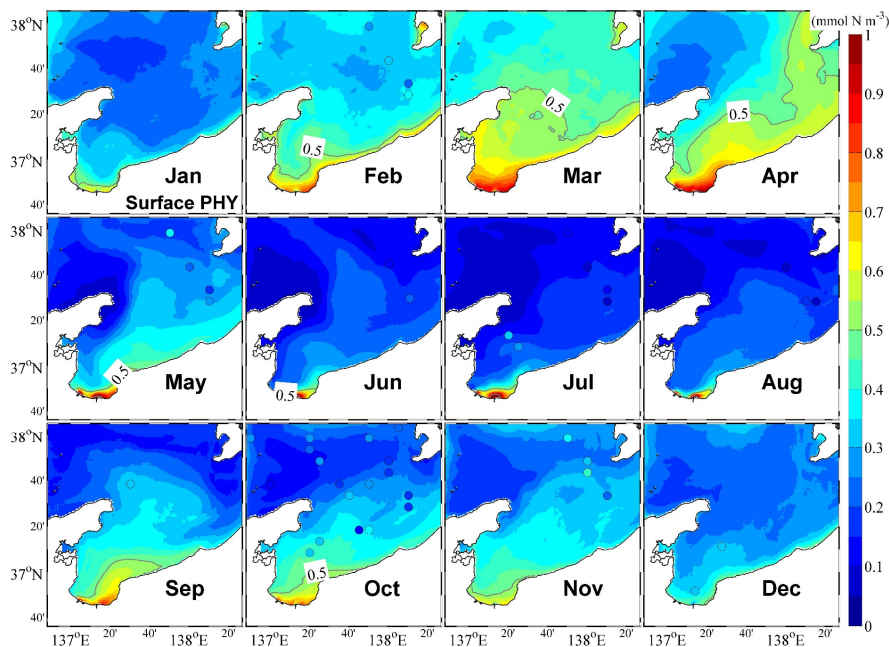
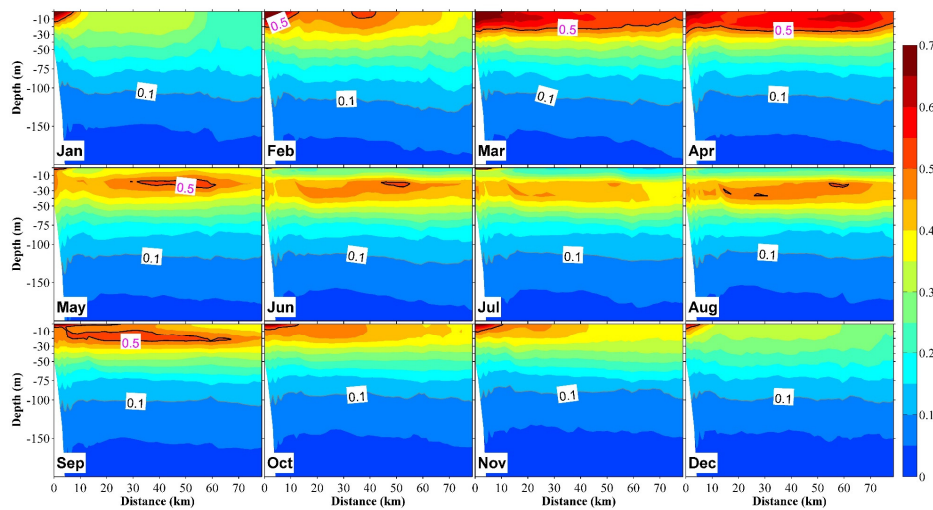


Figure 6: Monthly mean surface phytoplankton concentrations. The color circles represent observational data.

270

The distributions and seasonal variations of zooplankton are strongly dependent on the phytoplankton (Figures S6a and S6b). Similarly, the changes in detritus, which was derived from phytoplankton and zooplankton, coincide with the changes in phytoplankton, except that the concentrations of surface detritus are lower in shallower areas near the shore, possibly due to the sinking of detritus (Figures S7a and S7b).



275

Figure 7: Vertical distribution at section S2 (in Figure 1b) of phytoplankton in 12 months.



### 3.3 Contributions of different nutrient sources to total nutrient concentrations and primary production

Based on model results given by the tracking module, which enabled the distinction of nutrients originating from different sources, we evaluated the respective contributions of different nutrient sources to total nutrients and primary production. We found that nutrients derived from river water were predominantly distributed in the surface layer (0–20 m) of the inner coastal area of the bay. These river-derived nutrients spread out to the central part of the bay, reaching ~40 km from the shore (Figures 8 and S8). Further, these river-derived nutrients accounted for more than 50% of total nutrients close to the river mouths (Figure 8), and the seasonal variation of this proportion (Figures 8 and S8) was consistent with that of riverine nutrient loading (Figure 2c), which peaked in June and July.

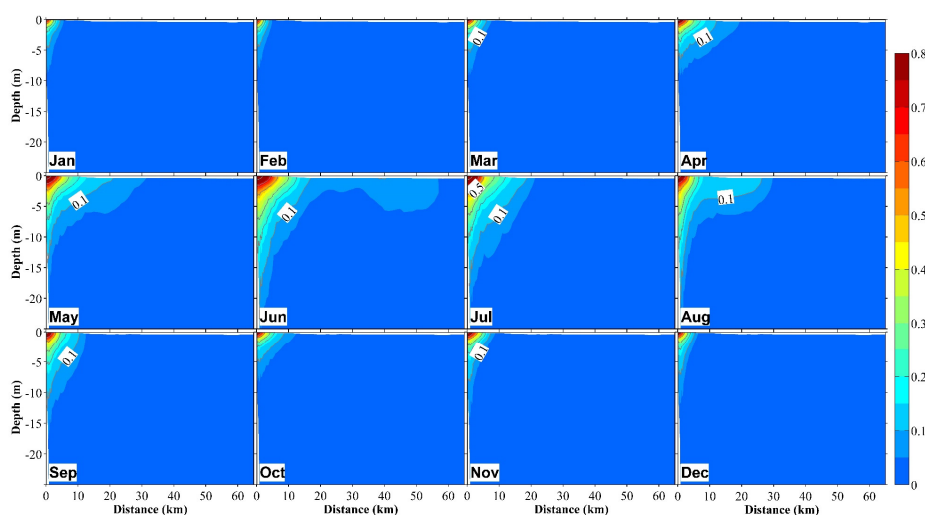


Figure 8: Vertical distribution at section S2 (Figure 1b) of the ratio of dissolved inorganic nitrogen originating from river water ( $DIN_{RV}$ ) to the total DIN in 12 months.

290

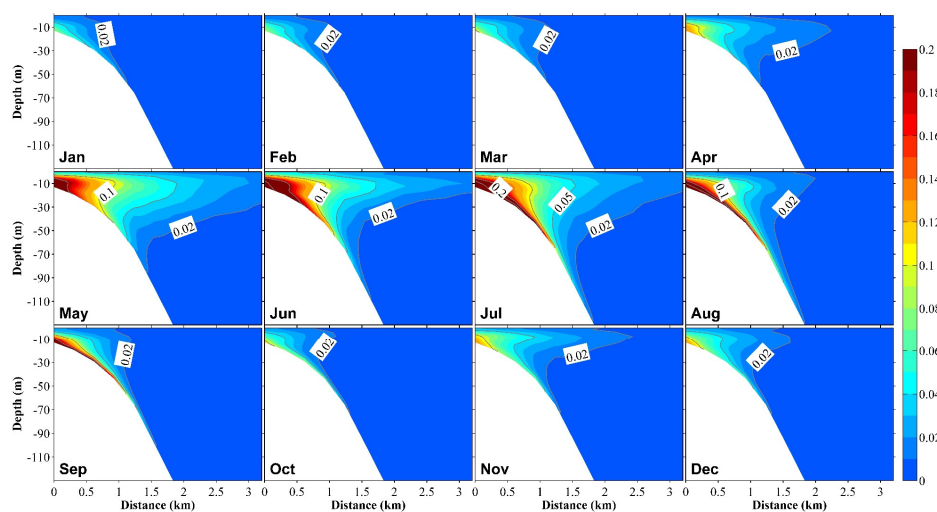
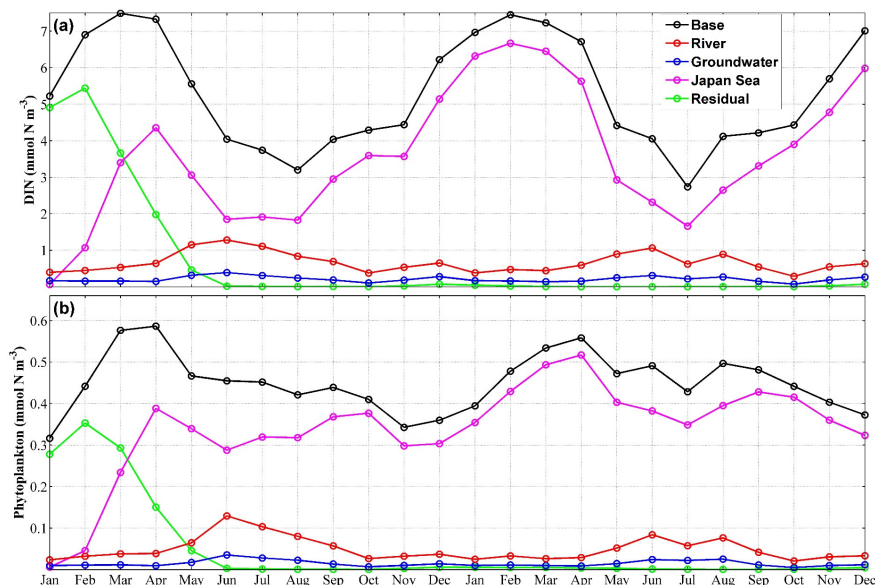


Figure 9: Vertical distributions at section S3 (Figure 1b) of the ratio of dissolved inorganic nitrogen originating from submarine groundwater discharge ( $DIN_{SGD}$ ) to the total DIN in 12 months.

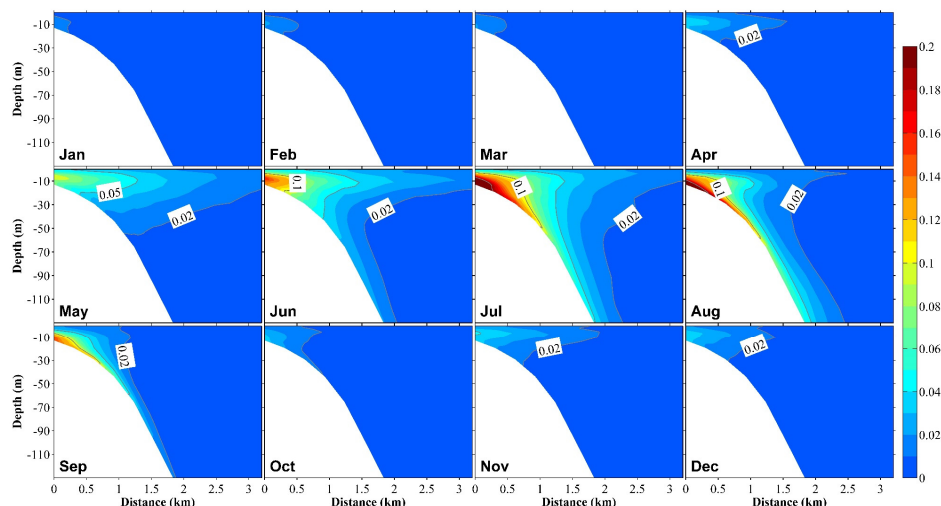


On the other hand, SGD-derived nutrients were primarily distributed in areas close to the coast within ~3 km from the shore, and they accounted for a smaller proportion of the total nutrients relative to river-derived nutrients; their maximum contribution to total nutrients close to the coast reached ~20% (Figures 9 and S9). Additionally, SGD-derived nutrients were not only abundant in the middle and bottom layers but also showed upward movement to the surface layer throughout the year (Figure 9). Similar to river-derived nutrients, SGD-derived nutrients showed their highest contribution to total nutrients in June and July (Figure 9). Except for the inner coastal areas, the nutrients from the Japan Sea dominated in the other areas (Figure S10). Given that nutrients derived from the landside (including river water and SGD) were found to be predominantly distributed in the inner coastal area, we divided the Toyama Bay area (Figure 1c) into two sub-areas, the shallow and deep water sub-areas, based on the 100-m isobath line, which is ~4 km away from the shore. Next, we calculated the volume-averaged DIN in each sub-area from a depth of 70 m to the surface for each nutrient source (Figure 10). In the shallow water sub-area, the volume-averaged concentration of total DIN was 5.52 mmolN m<sup>-3</sup>, while those derived from river water, SGD, and the Japan Sea were 0.61, 0.19, and 4.72 mmolN m<sup>-3</sup>, respectively. In the deep water sub-area, the volume-averaged concentrations of DIN derived from river water and SGD were very low, being 0.09 and 0.02 mmolN m<sup>-3</sup>, respectively, while the DIN from the Japan Sea had a mean value of 5.05 mmolN m<sup>-3</sup>. We also observed that the residual nutrients in the bay were generally consumed within the first half year (Figure 10), implying a fast water exchange process of the Bay with the Japan Sea.



310 **Figure 10: Two-year time series of the volume-averaged concentrations of dissolved inorganic nitrogen (DIN) (a) and phytoplankton (b) in the shallow water sub-area from a depth of 70 m to the surface for each nutrient source. ‘Base’ represents the total concentration, while ‘River’, ‘Groundwater’, ‘Japan Sea’, and ‘Residual’ represent the nutrient source of river water, groundwater, Japan Sea, and the residual nutrients.**

315 The ratio of phytoplankton supported by river-derived nutrients to total phytoplankton was slightly smaller than the ratio of river-derived nutrients to total nutrients; however, their distributions and seasonal variations were similar (Figures 10 and S11). The contributions of the SGD-derived nutrients to phytoplankton growth were also almost the same as their contributions to the total nutrients (Figure 11). In the shallow water sub-area, the volume-averaged concentration of total phytoplankton was 0.41 mmolN m<sup>-3</sup>, while the volume-averaged concentrations of phytoplankton supported by nutrients from different sources, i.e., river water, SGD, and the Japan Sea, were 0.05, 0.02, and 0.33 mmolN m<sup>-3</sup>, respectively (Figure 10). Furthermore, in the deep water sub-area, the volume-averaged concentrations of phytoplankton supported by landside-derived nutrients, including river water and SGD, decreased to a negligible value.



325 **Figure 11: Vertical distributions at section S3 (Figure 1b) of the proportions of phytoplankton supported by nutrients originating from submarine groundwater discharge ( $PHY_{SGD}$ ) to the total phytoplankton in 12 months.**

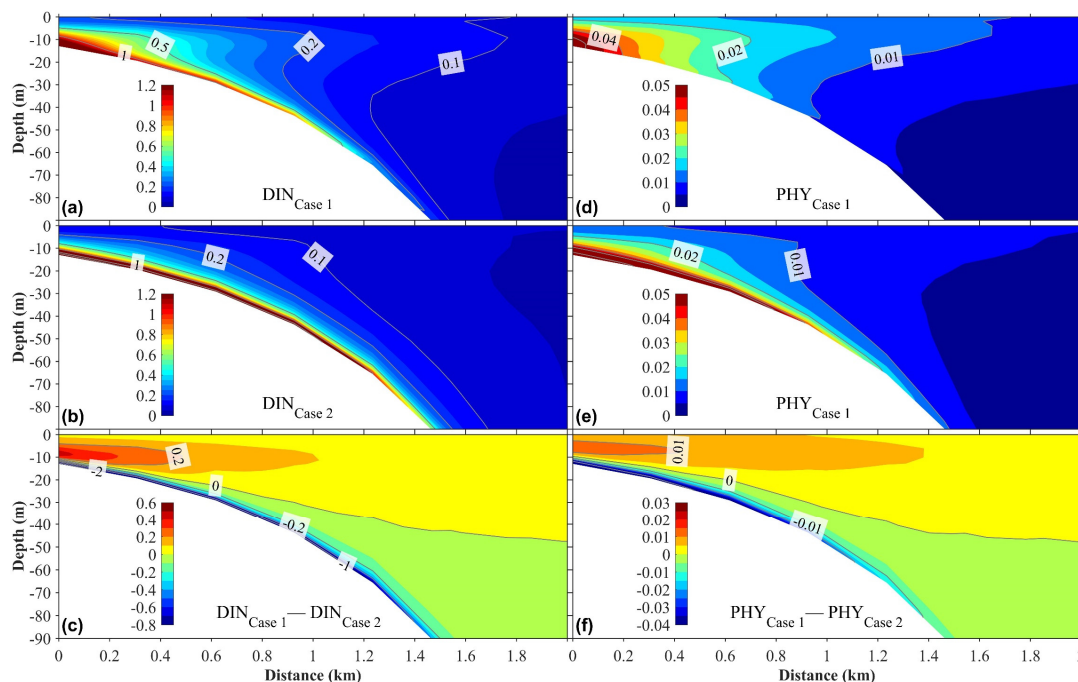
## 4 Discussion

### 4.1 Impact of the buoyancy effect of SGD on upward nutrient transport

As stated in Section 3.3, although SGD-derived DIN was released from the sea bottom, it can reach the surface layer. One possible mechanism responsible for this process is the buoyancy effect of SGD. The fresh SGD is lighter than surrounding seawater at the sea bottom and causes upward convection, which promotes the upward transport of nutrients from the sea bottom (Kreuzburg et al., 2023). To confirm its effect, we performed another simulation (Case 2), in which we removed the bottom salinity flux due to SGD in the hydrodynamic model but kept the SGD-derived DIN flux in the ecosystem model. For easy reference, we call the calculation with the bottom salinity flux due to SGD as Case 1.

330  
The upward vertical current was weaker in Case 2 than in Case 1 (Figure S12). Since most previous studies only estimated the amount of SGD (Hatta and Zhang, 2013; Luoma et al., 2021; Santos et al., 2009, 2021; Xu et al., 2024), we know little about its impact on the vertical current in the sea. The difference between the two calculations shows that the buoyancy effect of SGD can intensify the vertical velocity by about 0.1~0.2 mm/s (Figure S12). In addition, the salinity above the outlet location of SGD slightly decreased by 0.1 – 0.4 with the inclusion of bottom salinity flux due to SGD in Case 1 (Figure S12).

340  
With the weakening of the upward vertical current, the upward transport of SGD-derived nutrients was also weakened in Case 2 than in Case 1. Figure 12 shows the vertical distributions of the annual mean nutrients originating from SGD and their supported phytoplankton of Case 1 and Case 2, and the differences in the nutrients and phytoplankton between these two calculations. Without the buoyancy of SGD, the SGD-derived nutrients were mainly distributed from the sea bottom to the subsurface layer, and their distribution was almost absent in the surface layer (Figure 12). In Case 2, the SGD-derived nutrients were supplied to the surface layer only in winter. In addition, without the buoyancy effect of SGD, more nutrients spread away from the shallow water area in the bottom layer (Figure 12). Similarly, the phytoplankton supported by SGD-derived nutrients decreased in Case 2 (Figure 12).



350

**Figure 12:** (a) and (b) show the vertical distributions of annual mean dissolved inorganic nitrogen ( $DIN_{SGD}$ ) originating from submarine groundwater discharge (SGD) of calculations with (Case 1) and without (Case 2) buoyancy effect of SGD in the hydrodynamic model, and (c) shows the difference between them. Similarly, (d) and (e) mean the vertical distributions of annual mean phytoplankton ( $PHY_{SGD}$ ) supported by nutrients originating from SGD of calculations Case 1 and Case 2, and (f) shows the difference between them.

355

Our additional calculation shows that in a deep coastal sea, the buoyancy effect of SGD plays an important role in the upward transport of SGD-derived nutrients from the sea bottom. Without the buoyancy effect of SGD, it is difficult for these nutrients to reach the euphotic layer and be consumed by phytoplankton. Therefore, in addition to the wind-induced and tide-induced vertical mixing, the buoyancy effect of SGD is also an important mechanism for the upward transport of SGD-derived nutrients.

#### 4.2 Comparison of utilization between SGD-derived and riverine nutrients

360

Weather and how much SGD-derived nutrients can be used by phytoplankton should depend on the water depth because the concentration of SGD-derived nutrients generally decreases from the sea bottom to the sea surface. To evaluate the utilization of SGD-derived nutrients by the phytoplankton, we calculated the related material flows in four areas near the SGD outlet locations (Figure 1c) with different water depths, i.e., 0–20 (area 1), 20–70 (area 2), 70–200 (area 3), and 200–500 m (area 4) (Figure 13). The net biogeochemical consumption flux of DIN is defined as,

365

$$\begin{aligned}
 \text{Net biogeochemical processes of DIN} = \\
 -\text{photosynthesis} + \text{respiration} + \text{mineralization} + \text{excretion}.
 \end{aligned}
 \tag{6}$$

370

The annual mean transport of SGD-derived DIN into the bay is  $1925 \text{ mmol s}^{-1}$ . Since the 0–20 m area occupies part of the SGD outlet, the DIN transport into this area is  $433 \text{ mmol s}^{-1}$ . Among the biogeochemical processes, the consumption rates (photosynthesis) of SGD-derived DIN in the 4 areas from shallow to deep were 94, 120, 43, and  $70 \text{ mmol s}^{-1}$ , and the regeneration rates including respiration, excretion, and mineralization were 32, 65, 83, and  $119 \text{ mmol s}^{-1}$ , respectively (Figure 13). After excluding the vertical export flux of detritus (DET) to the sediment shown in Fig. 13, the horizontal transport of biological particles ( $PHY+ZOO+DET$ ) related to SGD-derived DIN is  $48 \text{ mmol s}^{-1}$  from area 1 to area 2,  $98 \text{ mmol s}^{-1}$  from



area 2 to area 3, 57  $\text{mmol s}^{-1}$  from area 3 to area 4, and 8  $\text{mmol s}^{-1}$  from area 4 to the further offshore area. Such a reduction in horizontal transport of the particles with the distance away from the coast is consistent with the reduction of utilization of SGD-derived DIN from area 1 to area 4. Apparently, with the increasing of water depth where SGD-derived DIN distributes from area 1 to area 4, it becomes difficult for SGD-derived nutrients to reach the euphotic layer and be consumed by phytoplankton (Fig. 13b).

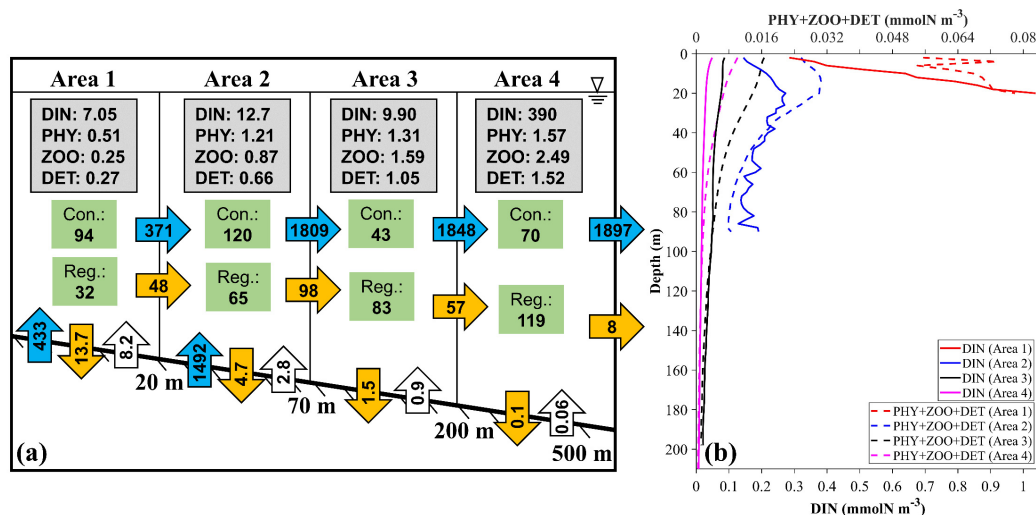


Figure 13: (a) The annual mean inventories and material flows of SGD-derived nutrients in 4 different areas near the outlet locations of SGD (Figure 1c). (Area 1) 0–20 m, (Area 2) 20–70 m, (Area 3) 70–200 m, (Area 4) 200–500 m. The values in the grey rectangles represent the inventory ( $\times 10^7 \text{ mmol}$ ) of the ecosystem variables in the area. The values in the green rectangles represent the consumption (Con.) and regeneration (Reg.) rates of  $\text{DIN}_{\text{GW}}$  in the biogeochemical processes ( $\text{mmol s}^{-1}$ ). The values in the vertical blue arrows represent the input transport of  $\text{DIN}_{\text{GW}}$  ( $\text{mmol s}^{-1}$ ). The values in the vertical orange and white arrows represent the vertical flux to the sediment and re-decomposition flux from the sediment to the sea ( $\text{mmol s}^{-1}$ ). The values in the horizontal blue and orange arrows represent the horizontal transport of  $\text{DIN}_{\text{GW}}$  and its related biological particles ( $\text{PHY}_{\text{GW}} + \text{ZOO}_{\text{GW}} + \text{DET}_{\text{GW}}$ ) ( $\text{mmol s}^{-1}$ ). (b) show the average profile of  $\text{DIN}_{\text{GW}}$ ,  $\text{PHY}_{\text{GW}}$ , and  $\text{DET}_{\text{GW}}$  in these 4 areas.

Similarly, we also calculated the material flow of river-derived nutrients in the 4 areas (Figure S13). Among the biogeochemical processes, the consumption rates of river-derived DIN in the 4 areas were 286, 235, 238, and 542  $\text{mmol s}^{-1}$  and the regeneration rates were 125, 168, 218, and 445  $\text{mmol s}^{-1}$ , respectively (Figure S13), all of which are larger than those related to SGD-derived DIN by several times. The horizontal transport of the biological particles ( $\text{PHY} + \text{ZOO} + \text{DET}$ ) supported by river-derived DIN was 114  $\text{mmol s}^{-1}$  from area 1 to area 2, 176  $\text{mmol s}^{-1}$  from area 2 to area 3, 194  $\text{mmol s}^{-1}$  from area 3 to area 4, and 291  $\text{mmol s}^{-1}$  from area 4 to the further offshore area. The biological activity related to river-derived DIN was kept and even increased from area 1 to area 4, and consequently, the proportion of riverine nutrients used by phytoplankton increased. Differing from the SGD-derived DIN that stayed in the deep layer, the river-derived DIN was mainly distributed in the surface layer (Fig. 13b) and therefore easily consumed by phytoplankton.

Currently, the impact of landside-derived nutrients (including SGD and rivers) on coastal marine ecosystems is usually evaluated by their nutrient loadings, without considering their respective distributions in the sea and whether they can be really used by the phytoplankton (Santos et al., 2021; Silverman et al., 2024). Our results show that due to the different distribution characteristics of nutrients originating from different sources (SGD and rivers), their impacts on the phytoplankton growth are different, and these impacts also vary with water depth. Additionally, in addition to the fresh SGD we studied here, there is another type of SGD in the seas that comes from saline SGD, i.e. recirculating seawater (Santos et al., 2021; Xu et al., 2024). The saline SGD are widely distributed in the seabed deeper than fresh SGD and release mostly recycled nutrients to global coastal waters (Santos et al., 2021). However, due to the lack of buoyancy in saline SGD and the deep location where it enters the sea, the nutrients derived from saline SGD would be more difficult than the fresh SGD to be transported upward and then





405 consumed by phytoplankton. Therefore, when evaluating the impact of SGD-derived nutrients on coastal marine ecosystems,  
it is necessary to consider not only the loading but also the distribution of SGD in which the fresh and saline SGDs are different.

## 5 Conclusions

In this study, we constructed a coupled physical-ecosystem model with a tracking module to evaluate the effects of SGD-derived nutrients as well as nutrients from other external sources on total nutrients and phytoplankton growth in Toyama Bay,  
410 where the SGD flow rates are greater than are observed in most other areas worldwide (Taniguchi et al., 2002; Zhang et al., 2005). The distributions and spatiotemporal characteristics of the impacts of these nutrients from different sources were clarified using the tracking results. Additionally, we clarified the seasonal variations in the total nutrient dynamics of Toyama Bay as well as its ecosystem structure and characteristics (Text S5).

Specifically, our model revealed that in this bay, nutrients derived from river water are predominantly distributed in the surface  
415 layer (0–20 m) close to river mouth areas, and their contribution to total nutrients was found to be ~50%. Conversely, SGD-derived nutrients were found to be primarily distributed in the areas close to the coast, and their contribution to total nutrient inventory was lower than that of river-derived nutrients. It was also found that SGD-derived nutrients released from the sea bottom were abundant in the middle and bottom layers and some of them could move upward to the surface layer. Comparison based on models with and without the salinity flux of SGD in the hydrodynamic model revealed that the upward transport of  
420 SGD-derived nutrients to the surface layer is primarily attributed to the buoyancy effect of SGD. The spatial distribution range of SGD-derived nutrients became smaller in the calculation results without the buoyancy effect of SGD, implying that the buoyancy effect of SGD cannot be ignored when evaluating the behavior of SGD-related nutrients.

The different distribution depths of river- and SGD-derived nutrients in the water column determine their contribution to the phytoplankton growth from the coastal to the offshore areas. The river-derived nutrients were surface-orientated and easily  
425 used by the phytoplankton in a larger area from the coast. In contrast, the SGD-derived nutrients were bottom-orientated and were not easily used by the phytoplankton. In the area close to the coast, the shallow water depth allows its use by the phytoplankton. With the distance away from the coast, it is gradually difficult for them to be used by the phytoplankton.

An important implication of this study is that the evaluation of the role of SGD-derived nutrients in the marine ecosystem cannot be based on the input amount of nutrients. A more reasonable way is based on how much nutrients can be used by the  
430 phytoplankton and enter the biogeochemical cycle of nutrients in the sea. This does not deny the importance of landside-derived nutrients to the marine ecosystem because the area affected by landside-derived nutrients usually is the spawning area of many marine organisms such as firefly squids, krills, and halfbeaks in the bay (Iguchi, 1995; Oya et al., 2002). In addition, the river discharge and SGD have not only seasonal variations but also short-term variations, to which we paid little attention in this study. In the future, we need a more comprehensive understanding of the influences of these landside-derived nutrients  
435 on the marine ecosystem by extending not only the biological species but also the time scales of temporal variations.

## Author contribution

MD developed the coupled physical-ecosystem model and performed the simulations. MD and XG prepared the manuscript. All the authors reviewed the manuscript.

440

## Competing interests

The contact author has declared that none of the authors has any competing interests.



### Acknowledgments

445 This work was supported by the Environment Research and Technology Development Fund (JPMEERF20212001) of the  
Environmental Restoration and Conservation Agency of Japan and a Grant-in-Aid for Scientific Research (MEXT KAKENHI,  
grant number: 22H05206). M. Dong was supported by the Ministry of Education, Culture, Sports, Science and Technology,  
Japan (MEXT) to a project on Joint Usage/Research Center–Leading Academia in Marine and Environment Pollution Research  
(LaMer).

450

### Data Availability Statement

The model results that support the findings of this study are available online at <https://doi.org/10.5281/zenodo.11075610>.

### References

- 445 Bratton, J. F.: The three scales of submarine groundwater flow and discharge across passive continental margins, *J. Geol.*,  
118, 565–575, <https://doi.org/10.1086/655114>, 2010.
- Burnett, W. C., Taniguchi, M., and Oberdorfer, J.: Measurement and significance of the direct discharge of groundwater into  
the coastal zone, *J. Sea Res.*, 46, 109–116, [https://doi.org/10.1016/S1385-1101\(01\)00075-2](https://doi.org/10.1016/S1385-1101(01)00075-2), 2001.
- Burnett, W. C., Bokuniewicz, H., Moore, W. S., and Taniguchi, M.: Groundwater and pore water inputs to the coastal zone,  
460 *Biogeochemistry*, 66, 3–33, 2003.
- Cho, H. M., Kim, G., Kwon, E. Y., Moosdorf, N., Garcia-Orellana, J., and Santos, I. R.: Radium tracing nutrient inputs  
through submarine groundwater discharge in the global ocean, *Sci. Rep.*, 8, 1–7, [https://doi.org/10.1038/s41598-018-20806-](https://doi.org/10.1038/s41598-018-20806-2)  
2, 2018.
- Church, T. M.: An Underground Route for the Water Cycle, *Nature*, 380, 579–580, 1996.
- 465 Cloern, J. E., Foster, S. Q., and Kleckner, A. E.: Phytoplankton primary production in the world’s estuarine-coastal  
ecosystems, *Biogeosciences*, 11, 2477–2501, <https://doi.org/10.5194/bg-11-2477-2014>, 2014.
- Fasham, M. J. R., Ducklow, H. W., and McKelvie, S. M.: A nitrogen-based model of plankton dynamics in the oceanic  
mixed layer, *J. Mar. Res.*, 48, 591–639, 1990.
- Guo, X. and Yanagi, T.: The Role of the Taiwan Strait in an Ecological Model in the East China Sea, *Acta Oceanogr.*  
470 *Taiwanica*, 37, 139–164, 1998.
- Hatta, M. and Zhang, J.: Temporal changes and impacts of submarine fresh groundwater discharge to the coastal  
environment: A decadal case study in Toyama Bay, Japan, *J. Geophys. Res. Ocean.*, 118, 2610–2622,  
<https://doi.org/10.1002/jgrc.20184>, 2013.
- Hatta, M., Zhang, J., Satake, H., Ishizaka, J., and Nakauchi, Y.: Water mass structure and fresh water fluxes (riverine and  
475 SGD’s) into Toyama Bay, *Chikyukagaku (Geochemistry)*, 39, 157–164, <https://doi.org/10.14934/chikyukagaku.39.157>,  
2005.
- Hwang, D.-W., Lee, Y.-W., and Kim, G.: Large submarine groundwater discharge and benthic eutrophication in Bangdu Bay  
on volcanic Jeju Island, Korea, *Limnol. Oceanogr.*, 50, 1393–1403, <https://doi.org/10.4319/lo.2005.50.5.1393>, 2005.



- Igeta, Y., Yankovsky, A., Fukudome, K. I., Ikeda, S., Okei, N., Ayukawa, K., Kaneda, A., and Watanabe, T.: Transition of  
480 the Tsushima Warm Current path observed over Toyama Trough, Japan, *J. Phys. Oceanogr.*, 47, 2721–2739,  
<https://doi.org/10.1175/JPO-D-17-0027.1>, 2017.
- Igeta, Y., Kuga, M., Yankovsky, A., Wagawa, T., Fukudome, K. I., Kaneda, A., Ikeda, S., Tsuji, T., and Hirose, N.: Effect  
of a current trapped by a continental slope on the pathway of a coastal current crossing Toyama Trough, Japan, *J. Oceanogr.*,  
77, 685–701, <https://doi.org/10.1007/s10872-021-00601-w>, 2021.
- 485 Iguchi, N.: Spring diel migration of a euphausiid *Euphausia pacifica* in Toyama Bay, southern Japan Sea, *Bull. Japan Sea  
Natl. Fish. Res. Inst.*, 45, 59–68, 1995.
- Ishizu, M., Miyazawa, Y., Tsunoda, T., and Guo, X.: Development of a biogeochemical and carbon model related to ocean  
acidification indices with an operational ocean model product in the North Western Pacific, *Sustainability*, 11, 2677,  
<https://doi.org/10.3390/su11092677>, 2019.
- 490 Jiao, J. and Post, V.: Submarine Groundwater Discharge, in: *Coastal Hydrogeology*, Cambridge University Press, 187–214,  
<https://doi.org/https://doi.org/10.1017/9781139344142>, 2019.
- Grid Point Value of Meso-Scale Model: <http://database.rish.kyoto-u.ac.jp/arch/jmadata/data/gpv/netcdf/MSM-S/>.
- Kawamiya, M.: Mechanism of offshore nutrient supply in the western Arabian Sea, *J. Mar. Res.*, 59, 675–696, 2001.
- Kondo, J.: Air-sea bulk transfer coefficients in diabatic conditions, *Boundary-Layer Meteorol.*, 9, 91–112, 1975.
- 495 Koyama, Y., Zhang, J., Hagiwara, T., Satake, H., and Asai, K.: Flow measurement of submarine groundwater discharge at  
wide area in the Eastern Toyama Bay, *Chikyukagaku (Geochemistry)*, 39, 149–155, 2005.
- Kreuzburg, M., Scholten, J., Hsu, F.-H., Liebetrau, V., SultenfuB, J., Rapaglia, J., and Schluter, M.: Submarine Groundwater  
Discharge-Derived Nutrient Fluxes in Eckernförde Bay (Western Baltic Sea), *Estuaries and Coasts*, 46, 1190–1207, 2023.
- Lapointe, B. E., O’Connell, J. D., and Garrett, G. S.: Nutrient couplings between on-site sewage disposal systems,  
500 groundwaters, and nearshore surface waters of the Florida Keys, *Biogeochemistry*, 10, 289–307, 1990.
- Lecher, A. L. and Mackey, K. R. M.: Synthesizing the effects of submarine groundwater discharge on Marine Biota,  
*Hydrology*, 5, 1–21, <https://doi.org/10.3390/hydrology5040060>, 2018.
- Leng, Q., Guo, X., Zhu, J., and Morimoto, A.: Contribution of the open ocean to the nutrient and phytoplankton inventory in  
a semi-enclosed coastal sea, *Biogeosciences*, 20, 4323–4338, <https://doi.org/https://doi.org/10.5194/bg-20-4323-2023>, 2023.
- 505 Luijendijk, E., Gleeson, T., and Moosdorf, N.: Fresh groundwater discharge insignificant for the world’s oceans but  
important for coastal ecosystems, *Nat. Commun.*, 11, 1–12, <https://doi.org/10.1038/s41467-020-15064-8>, 2020.
- Luoma, S., Majaniemi, J., Pullinen, A., Mursu, J., and Virtasalo, J. J.: Geological and groundwater flow model of a  
submarine groundwater discharge site at Hanko (Finland), northern Baltic Sea, *Hydrogeol. J.*, 29, 1279–1297,  
<https://doi.org/10.1007/s10040-021-02313-3>, 2021.
- 510 Matsuura, T. and Tebakari, T.: Impact of precipitation changes due to climate change on NO<sub>3</sub>-N in the Kurobe River,  
*Japanese Assoc. Groundw. Hydrol. 2022 Fall Lect.*, 192–196, 2022.
- Matsuura, T., Harada, K., and Tebakari, T.: Impact of the diffusion of public sewage systems in Toyama Prefecture on  
nitrogen loading in Toyama Bay, *Japanese Assoc. Groundw. Hydrol. 2023 Fall Lect.*, 24–27, 2023.
- Mellor, G. and Blumberg, A.: Wave breaking and ocean surface layer thermal response, *J. Phys. Oceanogr.*, 34, 693–698,  
515 <https://doi.org/10.1175/2517.1>, 2004.
- Mellor, G. L., Ezer, T., and Oey, L.-Y.: The Pressure Gradient Conundrum of Sigma Coordinate Ocean Models, *J. Atmos.  
Ocean. Technol.*, 11, 1126–1134, 1994.
- Ménesguen, A., Cugier, P., and Leblond, I.: A new numerical technique for tracking chemical species in a multisource,  
coastal ecosystem applied to nitrogen causing *Ulva* blooms in the Bay of Brest (France), *Limnol. Oceanogr.*, 51, 591–601,  
520 [https://doi.org/10.4319/lo.2006.51.1\\_part\\_2.0591](https://doi.org/10.4319/lo.2006.51.1_part_2.0591), 2006.
- MIRC: MIRC Ocean Dataset 2005 Documentation, 2005.



- Miyazawa, Y., Zhang, R., Guo, X., Tamura, H., Ambe, D., Lee, J. S., Okuno, A., Yoshinari, H., Setou, T., and Komatsu, K.: Water mass variability in the western North Pacific detected in a 15-year eddy resolving ocean reanalysis, *J. Oceanogr.*, 65, 737–756, <https://doi.org/10.1007/s10872-009-0063-3>, 2009.
- 525 Moore, W. S.: Large groundwater inputs to coastal waters revealed by 226Ra enrichments, *Nature*, 380, 612–614, 1996.  
Moore, W. S.: The effect of submarine groundwater discharge on the ocean, *Ann. Rev. Mar. Sci.*, 2, 59–88, <https://doi.org/10.1146/annurev-marine-120308-081019>, 2010.
- Müller, T., Gros, J., Leibold, P., Al-Balushi, H., Petermann, E., Schmidt, M., Brückmann, W., Al Kindi, M., and Al-Abri, O. S.: Autonomous Large-Scale Radon Mapping and Buoyant Plume Modeling Quantify Deep Submarine Groundwater Discharge: A Novel Approach Based on a Self-Sufficient Open Ocean Vehicle, *Environ. Sci. Technol.*, 57, 6540–6549, <https://doi.org/10.1021/acs.est.3c00786>, 2023.
- Nakada, S., Isoda, Y., and Uchiyama, I.: Seasonal variations of water properties and the baroclinic flow pattern in Toyama Bay under the influence of the Tsushima Warm Current, *J. Oceanogr.*, 61, 943–952, <https://doi.org/10.1007/s10872-006-0011-4>, 2005.
- 535 Nakaguchi, Y., Yamaguchi, Y., Yamada, H., Zhang, J., Suzuki, M., Koyama, Y., and Hayashi, K.: Characterization and origin of chemical components in the submarine groundwater discharge in Toyama Bay, *Chikyukagaku (Geochemistry)*, 39, 119–130, 2005.
- Neumann, T.: The fate of river-borne nitrogen in the Baltic Sea—an example for the River Oder., *Estuar. Coast. Shelf Sci.*, 73, 1–7, 2007.
- 540 Onitsuka, G. and Yanagi, T.: Differences in ecosystem dynamics between the Northern and Southern parts of the Japan Sea: Analyses with two ecosystem models, *J. Oceanogr.*, 61, 415–433, <https://doi.org/10.1007/s10872-005-0051-1>, 2005.
- Onitsuka, G., Yanagi, T., and Yoon, J. H.: A numerical study on nutrient sources in the surface layer of the Japan Sea using a coupled physical-ecosystem model, *J. Geophys. Res. Ocean.*, 112, 1–17, <https://doi.org/10.1029/2006JC003981>, 2007.
- Oya, F., Tsuji, T., and Fujiwara, S.: Relative Growth and Feeding Habits of Halfbeak, *Hyporhamphus sajori*, Larvae and Juveniles in Toyama Bay of the Japan Sea, *Aquac.*, 50, 47–54, 2002.
- 545 Paulson, C. A. and Simpson, J. J.: Irradiance Measurements in the Upper Ocean, *J. Phys. Oceanogr.*, 7, 952–956, 1977.
- Redfield, A. C., Ketchum, B. H., and Richards, F. A.: The influence of organisms on the composition of seawater, in: *The Sea*, edited by: Hill, M. N., Interscience Publishers, New York, 26–77, 1963.
- Rodellas, V., Garcia-Orellana, J., Masqué, P., Feldman, M., Weinstein, Y., and Boyle, E. A.: Submarine groundwater discharge as a major source of nutrients to the Mediterranean Sea, *Proc. Natl. Acad. Sci. U. S. A.*, 112, 3926–3930, <https://doi.org/10.1073/pnas.1419049112>, 2015.
- 550 Rosati, A. and Miyakoda, K.: A General Circulation Model for Upper Ocean Simulation, *J. Phys. Oceanogr.*, 18, 1601–1626, 1988.
- Santos, I. R., Burnett, W. C., Chanton, J., Dimova, N., and Peterson, R. N.: Land or ocean?: Assessing the driving forces of submarine groundwater discharge at a coastal site in the gulf of mexico, *J. Geophys. Res. Ocean.*, 114, 1–11, <https://doi.org/10.1029/2008JC005038>, 2009.
- 555 Santos, I. R., Chen, X., Lecher, A. L., Sawyer, A. H., Moosdorf, N., Rodellas, V., Tamborski, J., Cho, H. M., Dimova, N., Sugimoto, R., Bonaglia, S., Li, H., Hajati, M. C., and Li, L.: Submarine groundwater discharge impacts on coastal nutrient biogeochemistry, *Nat. Rev. Earth Environ.*, 2, 307–323, <https://doi.org/10.1038/s43017-021-00152-0>, 2021.
- 560 Silverman, J., Strauch-Goza, S., and Asfur, M.: The Influence of Fresh Submarine Groundwater Discharge on Seawater Acidification Along the Northern Mediterranean Coast of Israel, *J. Geophys. Res. Ocean.*, 129, 1–21, <https://doi.org/10.1029/2024JC021010>, 2024.



- Sugimoto, R., Kitagawa, K., Nishi, S., Honda, H., Yamada, M., Kobayashi, S., Shoji, J., Ohsawa, S., Taniguchi, M., and Tominaga, O.: Phytoplankton primary productivity around submarine groundwater discharge in nearshore coasts, *Mar. Ecol. Prog. Ser.*, 563, 25–33, <https://doi.org/10.3354/meps11980>, 2017.
- 565 Taniguchi, M., Burnett, W. C., Cable, J. E., and Turner, J. V.: Investigation of submarine groundwater discharge, *Hydrol. Process.*, 16, 2115–2129, <https://doi.org/10.1002/hyp.1145>, 2002.
- Taylor, G. T., Gobler, C. J., and Sañudo-Wilhelmy, S. A.: Speciation and concentrations of dissolved nitrogen as determinants of brown tide *Aureococcus anophagefferens* bloom initiation, *Mar. Ecol. Prog. Ser.*, 312, 67–83, <https://doi.org/10.3354/meps312067>, 2006.
- 570 Varlamov, S., Miyazawa, Y., and Guo, X.: Regional nested tide-resolving real-time JCOPET modeling system for coastal waters of southern Japan, in: 2nd International Workshop on Modeling the Ocean (IWMO), 2010.
- Wang, S.-L., Chen, C.-T. A., Huang, T.-H., Tseng, H.-C., Lui, H.-K., Peng, T.-R., Kandasamy, S., Zhang, J., Yang, L., Gao, X., Lou, J.-Y., Kuo, F.-W., Chen, X.-G., Ye, Y., and Lin, Y.-J.: Submarine Groundwater Discharge helps making nearshore waters heterotrophic, *Sci. Rep.*, 8, 1–10, <https://doi.org/10.1038/s41598-018-30056-x>, 2018.
- 575 Wang, X., Du, J., Ji, T., Wen, T., Liu, S., and Zhang, J.: An estimation of nutrient fluxes via submarine groundwater discharge into the Sanggou Bay—A typical multi-species culture ecosystem in China, *Mar. Chem.*, 167, 113–122, <https://doi.org/https://doi.org/10.1016/j.marchem.2014.07.002>, 2014.
- Watanabe, Y., Matsuura, T., and Chiba, H.: Variability of summer water-mass structure in Toyama bay coastal-zone, *Oceanogr. Japan*, 22, 97–117, [https://doi.org/https://doi.org/10.5928/kaiyou.22.4\\_97](https://doi.org/https://doi.org/10.5928/kaiyou.22.4_97), 2013.
- 580 Xu, H., Xu, B., Yu, H., Zhao, S., Burnett, W. C., Yao, Q., Dimova, N. T., Song, S., Guo, X., Chen, X., Zhang, H., and Yu, Z.: Deciphering Multi-Scale Submarine Groundwater Discharge in a Typical Eutrophic Bay, *J. Geophys. Res. Ocean.*, 129, 1–15, <https://doi.org/10.1029/2024JC021042>, 2024.
- Zektser, I. S.: *Groundwater and the environment: applications for the global community*, edited by: Everett, L. G., Lewis Publishers, 175 pp., 2000.
- 585 Zhang, J. and Satake, H.: The chemical characteristics of submarine groundwater seepage in toyama bay, Central Japan, edited by: Taniguchi, M., Wang, K., and Gamo, T., Elsevier B.V., 45–60 pp., <https://doi.org/10.1016/B978-044451479-0/50016-9>, 2003.
- Zhang, J., Hagiwara, T., Koyama, Y., Satake, H., Nakamura, T., and Asai, K.: A new flow rate measuring method - SGD (submarine groundwater discharge) flux chamber and its approach off Katakai Alluvial Fan, Toyama Bay, Central Japan, *Chikyukagaku (Geochemistry)*, 39, 141–148, 2005.
- 590 Zhang, J., Guo, X., and Zhao, L.: Tracing external sources of nutrients in the East China Sea and evaluating their contributions to primary production, *Prog. Oceanogr.*, 176, 102122, <https://doi.org/10.1016/j.pocean.2019.102122>, 2019.
- Zhang, Y., Santos, I. R., Li, H., Wang, Q., Xiao, K., Guo, H., and Wang, X.: Submarine groundwater discharge drives coastal water quality and nutrient budgets at small and large scales, *Geochim. Cosmochim. Acta*, 290, 201–215, <https://doi.org/10.1016/j.gca.2020.08.026>, 2020.